

# DeepFusionCDR: Employing Multi-Omics Integration and Molecule-Specific Transformers for Enhanced Prediction of Cancer Drug Responses

Xiaowen Hu , Graduate Student Member, IEEE, Pan Zhang , Jiaxuan Zhang, and Lei Deng 

**Abstract**—Deep learning approaches have demonstrated remarkable potential in predicting cancer drug responses (CDRs), using cell line and drug features. However, existing methods predominantly rely on single-omics data of cell lines, potentially overlooking the complex biological mechanisms governing cell line responses. This paper introduces DeepFusionCDR, a novel approach employing unsupervised contrastive learning to amalgamate multi-omics features, including mutation, transcriptome, methylome, and copy number variation data, from cell lines. Furthermore, we incorporate molecular SMILES-specific transformers to derive drug features from their chemical structures. The unified multi-omics and drug signatures are combined, and a multi-layer perceptron (MLP) is applied to predict IC<sub>50</sub> values for cell line-drug pairs. Moreover, this MLP can discern whether a cell line is resistant or sensitive to a particular drug. We assessed DeepFusionCDR's performance on the GDSC dataset and juxtaposed it against cutting-edge methods, demonstrating its superior performance in regression and classification tasks. We also conducted ablation studies and case analyses to exhibit the effectiveness and versatility of our proposed approach. Our results underscore the potential of DeepFusionCDR to enhance CDR predictions by harnessing the power of multi-omics fusion and molecular-specific transformers. The prediction of DeepFusionCDR on TCGA patient data and case study highlight the practical application scenarios of DeepFusionCDR in real-world environments.

**Index Terms**—Multi-omics feature fusion, unsupervised learning, molecular smiles-specific transformers, cancer drug response (CDR) prediction.

Received 2 August 2023; revised 18 March 2024 and 16 May 2024; accepted 12 June 2024. Date of publication 27 June 2024; date of current version 4 October 2024. This work was supported by the National Natural Science Foundation of China under Grant U23A20321 and Grant 62272490. (*Corresponding author: Lei Deng*.)

Xiaowen Hu and Lei Deng are with the School of Computer Science and Engineering, Central South University, Changsha 410083, China (e-mail: altriaivin@163.com; leideng@csu.edu.cn).

Pan Zhang is with the Hunan Provincial Key Laboratory of Clinical Epidemiology, Xiangya School of Public Health, Central South University, Changsha 410078, China (e-mail: paulazhang@csu.edu.cn).

Jiaxuan Zhang is with the Department of Electrical and Computer Engineering, University of California, San Diego 92092 USA (e-mail: zhang.jiz69@gmail.com).

Source code and datasets can be available on <https://github.com/altriaivin/DeepFusionCDR>.

Digital Object Identifier 10.1109/JBHI.2024.3417014

## I. INTRODUCTION

CANCER, as a substantial global health concern, is impacting an increasingly younger demographic as substantiated by Cao et al. [1]. The innate heterogeneity of cancer poses substantial hurdles in the pursuit of precision treatment. Patients with identical types of cancer can demonstrate varied responses to anti-cancer drugs. However, the proliferation of publicly accessible drug screening datasets, such as the Cancer Cell Line Encyclopedia (CCLE) [2] and the Genomics of Drug-Sensitivity in Cancer (GDSC) project [3], has expedited advances in drug screening and repurposing.

In recent years, the advent of multi-omics data in cancer research has provided an opportunity to delve into the effects of tumor omics traits on drug responses [4]. Numerous data types, including genomic, transcriptomic, and methylomic data, have demonstrated potential in predicting drug responses [5], [6], [7], [8]. Transcriptome profiling, in particular, excels in capturing shifts in gene activity and regulation, quantifying expression patterns, and providing comprehensive portraits of underlying phenotypes [9]. Crucially, modifications in gene activity can function as phenotypic markers for apoptosis [10] and proliferation [11], both of which drastically influence critical clinical variables like metastatic potential [12] and treatment outcomes [13]. Therefore, the thorough integration of multi-omics data harbors significant potential for bolstering the precision of cancer drug response prediction.

The abundance of freely accessible, high-quality data has spurred a surge in the use of deep learning methods for predicting CDR. Existing studies largely fall into two categories. The first includes network-based methods, based on the premise that drugs with similar properties are likely associated with similar cell lines. Researchers construct networks of drug similarity and cell line similarity and derive information from these for CDR prediction [14], [15], [16]. However, these network-based methods tend to be unstable and computationally demanding. The second category encompasses machine learning-based methods, which directly interrogate the profiles of a vast array of drugs and cancer cell lines for CDR prediction [8], [17], [18], [19]. These methods predominantly extract cell line representations from single-omics features of the cell lines and sometimes employ molecular fingerprint features [7], [20] to characterize drugs.

These approaches, however, are not necessarily conducive to obtaining optimal feature representations. In recent years, a push towards extracting superior representations of cell lines and drugs from multi-omics features of drugs' SMILES and cell lines has been observed, using deep learning methods. For instance, techniques like tCNNs [8] leverage convolutional neural networks (CNNs) to distill drug features from SMILE structures. In contrast, GraphCDR [21] formulates a graph from the two-dimensional structure of drug molecules and applies graph convolutional network techniques for feature extraction. Similarly, methods such as ESPF [22] and DeepTTA [23] dissect the drug's SMILE into substructures and harness the transformer architecture [24] for drug feature extraction. Concurrently, DeepCDR [5] employs a unified graph convolutional network to represent drugs based on their chemical structure.

Despite the satisfactory results achieved, current methods still have scope for improvement. For drug feature extraction, the Transformer architecture shows promise, but treating SMILE as a simple sequence fails to fully exploit the two-dimensional structure and molecular distance information of drug molecules, thus limiting the quality of drug feature representations. In the extraction of multi-omics features, the prevalent practice of extracting and concatenating features from different omics types in a straightforward manner overlooks the potential interplay and complementarity among them. This approach hampers the extraction of more informative cell line feature representations. Moreover, in CDR prediction, most methods independently preprocess and concatenate cell line and drug feature representations and then train a classifier. The independent nature of these modules can lead to misalignment during model training, preventing the simultaneous optimization of both modules and restricting the overall enhancement of CDR prediction performance.

To surmount these limitations, we propose DeepFusionCDR, a novel method for cancer drug response prediction. DeepFusionCDR enhances the attention mechanism within the Transformer model by integrating inter-atomic distances and molecular graph structure, facilitating the extraction of more comprehensive and effective drug feature representations. For cell line feature extraction, we employ a unsupervised contrastive learning pre-training strategy to leverage multi-omics feature data and use a decoder to reconstruct fused features. Cancer drug response prediction is then carried out using a multilayer perceptron (MLP). Our experiments validate the superiority of DeepFusionCDR, demonstrating state-of-the-art performance in both classification and regression tasks. Ablation experiments further affirm the advantages of utilizing multi-omics features and contrastive learning, enabling the extraction of more informative cell line features that considerably enhance cancer drug response prediction. Case studies underscore the effectiveness of DeepFusionCDR, positioning it as a valuable tool for advancing cancer drug discovery and prevention.

## II. DATASET

In this study, we assessed DeepFusionCDR using both classification and regression tasks. For the regression task, we primarily used IC50 values for cell line-drug pairs from the

GDSC database [3] and CCLE database [2]. We downloaded multiple omics features of cell lines from both the GDSC and CCLE databases, and then selected cell lines that concurrently possessed CNV, gene mutation, transcriptomics, and methylation features, and had drug SMILE strings available in PubChem.

The transcriptomics analysis involved applying RMA normalization to RNA data, while methylation assessment used pre-processed CpG islands'  $\beta$ -values. We encoded gene mutation data in binary format and represented copy number variation (CNV) data ternary format, designating gene loss, normal copy number, and gene gain as -1, 0, and 1, respectively. As a result, we compiled a dataset consisting of 68,996 IC50 value pairs between 489 cell lines and 297 drugs.

For the classification task, following the methodologies of DeepCDR and DeepTTA, we binarized the IC50 values for each drug using the thresholds provided by Iorio et al. As some drugs lacked thresholds, we ended up with 1,819 instances classified as sensitive and 24,988 instances classified as resistant. We subsequently divided the data randomly into three subsets at ratios of 1:1, 1:5, and 1:10, respectively. These subsets were then utilized to evaluate the classification performance of DeepFusionCDR.

## III. METHODS

### A. Overview of DeepFusionCDR Framework

Fig. 1 illustrates the overall architecture of DeepFusionCDR, which is designed to incorporate drug SMILES and multi-omics data from cell lines. Its objective is to yield the IC50 value for a given cell line-drug pair or to predict whether the cell line is sensitive or resistant to the drug. The model comprises three principal components: cell line feature extraction, drug feature extraction, and prediction module. In the cell line feature extraction module, we utilize a pre-training strategy grounded in unsupervised contrastive learning to amalgamate multi-omics features. An encoder-decoder structure is employed to procure the fused embedding. In the drug feature extraction segment, we apply a molecule-specific transformer to glean the drug's embedding from its chemical structure, thereby capturing crucial characteristics of the drug molecule, which supports the prediction process. Finally, in the prediction module, the drug embedding is merged with the cell line embedding. By training a classifier or regression model on this combined representation, the model can perform precise classification or regression predictions for drug sensitivity or resistance. Thus, through these interconnected components, DeepFusionCDR ensures a comprehensive amalgamation of multi-omics data and drug features, enhancing predictions for cell line-drug interactions.

### B. Drug Feature Mining Module

In recent years, natural language processing (NLP) has become a powerful tool for textual data analysis, playing a significant role in advancing cheminformatics [25], [26]. Cheminformatics deals with the representation and manipulation of chemical structures and properties. The successful application of NLP in cheminformatics can be partially attributed to the common characteristics between these two fields, such as the

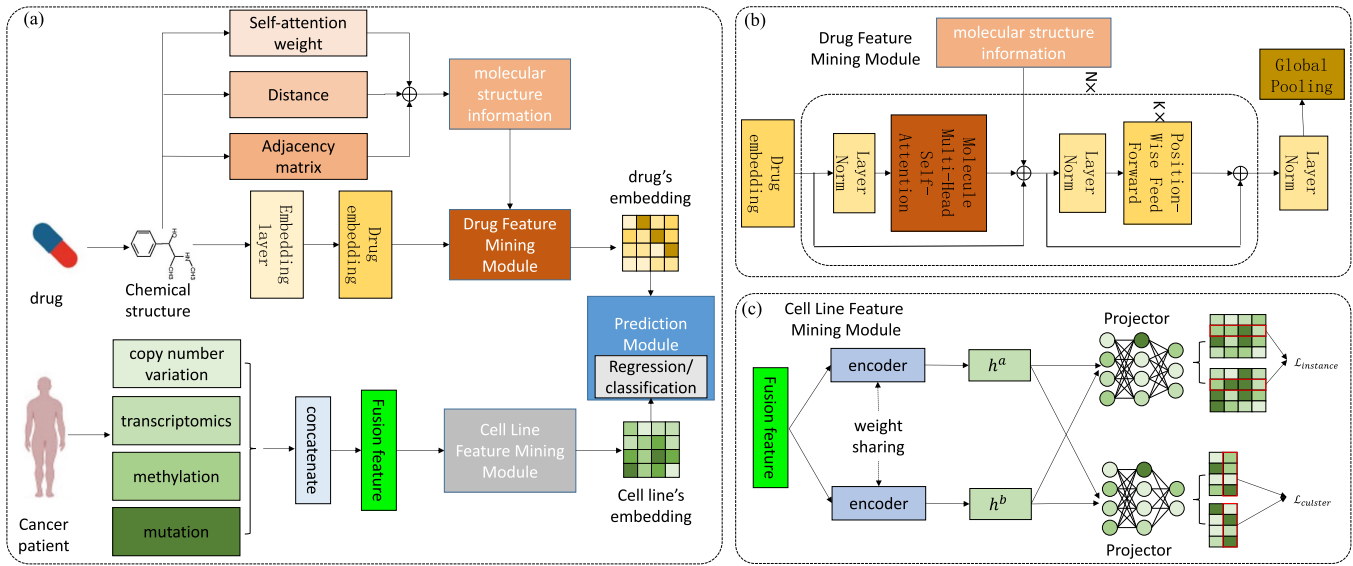


**Fig. 1.** (a) The main process of DeepFusionCDR involves the following steps. DeepFusionCDR takes multi-omics features of cell lines and drug SMILES as inputs. It employs drug feature extraction module and cell line feature extraction module to separately obtain drug features and cell line features. Subsequently, the acquired cell line features and drug features are concatenated and fed into an MLP classifier to predict the IC50 scores of drug-cell line pairs and determine whether the cell lines are resistant or sensitive to the drugs. (b) Drug Feature Mining Module: A molecule-specific transformer is utilized to extract drug features. (c) Cell Line Feature Mining Module: The cell line's multi-omics features are fused using unsupervised pre-training approach, and a decoder is employed to obtain the final fused cell line features.

use of graphs, sequences, and embeddings to model complex data [27].

The initial transformer architecture consisted of  $N$  attention blocks with multi-head self-attention, feed-forward layers, and a pooling layer. Each attention head, denoted as  $i$ , computed  $Q_i = HW_i^Q$ ,  $K_i = HW_i^K$ , and  $V_i = HW_i^V$  from the input  $H$ , which were subsequently utilized in the attention function described as follows:

$$\begin{cases} \text{head}_i = \text{softmax}\left(\frac{Q_i K_i^T}{\sqrt{d_k}} V_i\right) \\ \text{MultiHead}(Q, K, V) = \text{Concat}(\text{head}_1, \dots, \text{head}_h) W^O \end{cases} \quad (1)$$

where  $W_i^Q$ ,  $W_i^K$ ,  $W_i^V$  and  $W^O$  are the trainable parameters.

However, rather than employing the naive Transformer architecture to represent chemical molecules as sentences, we adopted the approach proposed by [28], which interprets self-attention as a soft adjacency matrix among elements in the input sequence. Inspired by this concept, we enhanced the self-attention mechanism by incorporating information about the actual molecular structure, thereby eschewing the need for linearized (textual) representations of molecules as input [27]. We posit that this offers a more favorable inductive bias for the model. To elaborate, we introduced the molecular self-attention layer, as defined in (2), replacing the original self-attention layer. The self-attention matrix was augmented using the following procedure: We let  $A \in \{0, 1\}^{N_{\text{atoms}} \times N_{\text{atoms}}}$  represent the graph adjacency matrix and  $D \in \mathbb{R}^{N_{\text{atoms}} \times N_{\text{atoms}}}$  denote the inter-atomic distances. Furthermore, we assigned  $\lambda_a$ ,  $\lambda_d$ , and  $\lambda_g$  as scalar weights corresponding to the self-attention, distance, and adjacency matrices, respectively. We then modified (1)

as follows:

$$E_{\text{drug}} = \left( \lambda_a \text{softmax}\left(\frac{Q_i K_i^T}{\sqrt{d_k}}\right) + \lambda_d g(D) + \lambda_g A \right) V_i \quad (2)$$

Here,  $\lambda_a$ ,  $\lambda_b$ , and  $\lambda_c$  serve as hyperparameters to balance the contribution of the three components.  $g(\cdot)$  denotes the softmax function, while  $D$  is obtained from the RDKit package.

### C. Cell Line Feature Mining Module

Contrastive learning is an efficient unsupervised learning approach that seeks to map raw data into a feature space, maximizing the similarity between positive pairs and minimizing it between negative pairs. Recently, contrastive learning has yielded remarkable results in computer vision [29], [30], [31], natural language processing [32], [33], and bioinformatics [34]. Encouraged by these successes, we decided to use unsupervised contrastive learning methods for preprocessing multi-omics features, employing a decoder to generate fused cell line features for cancer drug response prediction.

**1) Data Augmentation:** In processing the multi-omics features of each cell line, we first concatenated the four types of features to derive the fused feature,  $x_i$ . We then independently applied three distinct data augmentation methods to  $x_i$ , each with a certain probability, to generate augmented data,  $x_i^a$  and  $x_i^b$ . These augmentations included the addition of standard Gaussian noise to  $x_i$ , as well as the random masking or dropout of some elements of  $x_i$  by setting them to zero. We used two encoders with shared parameters to extract embeddings from  $x_i^a$  and  $x_i^b$ ,

represented as follows:

$$\begin{cases} h_i^a = f(x_i^a) \\ h_i^b = f(x_i^b) \end{cases} \quad (3)$$

Here,  $f(\cdot)$  signifies the encoder function. For our specific application, we used a four-layer deep neural network (DNN).

**2) Instance-Based Contrastive Learning Paradigm:** For each mini-batch, we employed a projector, denoted as  $g_{\text{Instance}}(\cdot)$ , to map the embeddings, which were extracted by the encoder, into the same feature space. This can be represented as:

$$\begin{cases} z_i^a = g_{\text{Instance}}(h_i^a) \\ z_i^b = g_{\text{Instance}}(h_i^b) \end{cases} \quad (4)$$

Adhering to an instance-based contrastive learning paradigm, we identify two samples that have been augmented from the same instance as positive pairs, while the remaining samples in each mini-batch are treated as negative pairs. Formally, given a mini-batch of  $N$  samples, denoted as  $x_1, \dots, x_N$ , we perform data augmentation on each sample  $x_i$  to produce  $2N$  augmented samples  $x_1^a, \dots, x_N^a, x_1^b, \dots, x_N^b$ . For any augmented sample  $x_i^a$ , its counterpart  $x_i^b$  is identified as a positive pair, denoted as  $x_i^a, x_i^b$ , and the remaining  $2N - 2$  augmented samples are treated as negative pairs.

According to InfoNCE, the contrastive learning loss for the instance-based contrastive learning loss, denoted as  $\mathcal{L}_{\text{instance}_i}^k$ , can be obtained as follows:

$$-\log \frac{\exp(s(z_i^a, z_i^b)/\tau)}{\sum_{j=1}^N [\exp(s(z_i^k, z_j^k)/\tau) + \exp(s(z_i^a, z_j^b)/\tau)]} \quad (5)$$

where  $\tau$  represents the temperature parameter that controls the softness, and  $k \in \{a, b\}$ . Here,  $s(x, y)$  calculates the cosine distance, which measures the similarity between two samples  $x$  and  $y$ , as follows:

$$s(x, y) = \frac{x \cdot y^T}{\|x\| \cdot \|y\|} \quad (6)$$

However, InfoNCE suffers from a significant negative-positive coupling effect that affects learning efficiency with respect to the batch size [35]. To address this issue, we employ the decoupled contrastive learning objective [35]. It excludes positive pairs from the denominator, yielding the instance-based contrastive learning loss, denoted as  $\mathcal{L}_{\text{instance}_i}^k$ , which can be formulated as follows:

$$-\log \frac{\exp(s(z_i^a, z_i^b)/\tau)}{\sum_{j=1, j \neq i}^N [\exp(s(z_i^k, z_j^k)/\tau) + \exp(s(z_i^a, z_j^b)/\tau)]} \quad (7)$$

Wherein, (7) can be simplified as follows:

$$-s(z_i^a, z_i^b) + \log \sum_{j=1, j \neq i}^N [\exp(s(z_i^k, z_j^k)/\tau) + \exp(s(z_i^a, z_j^b)/\tau)] \quad (8)$$

Next, we calculate a decoupled instance-level contrastive loss for each augmented sample to identify all positive pairs across the dataset. The overall contrastive learning loss for the instance-based contrastive learning paradigm is given by:

$$\mathcal{L}_{\text{instance}} = \frac{1}{2N} \sum_{i=1}^N (\mathcal{L}_{\text{instance}_i}^a + \mathcal{L}_{\text{instance}_i}^b) \quad (9)$$

**3) Cluster-Based Contrastive Learning Paradigm:** Taking inspiration from the “label as representation” principle in contrastive clustering [36], we map a data sample into a feature space of specific dimensions. The  $i$ -th element of this feature vector indicates the probability of the sample belonging to the  $i$ -th cluster, thereby representing its soft labels.

Building on this concept, we put forward a cluster-based contrastive learning paradigm. Firstly, we project the embeddings into a shared representation space using the following formula:

$$\begin{cases} y_i^a = g_{\text{cluster}}(h_i^a) \\ y_i^b = g_{\text{cluster}}(h_i^b) \end{cases} \quad (10)$$

Here,  $y_i^a$  and  $y_i^b$  represent the soft labels of samples  $x_i^a$  and  $x_i^b$ , respectively. Similar to the instance-based contrastive learning paradigm, we regard the augmented samples originating from the same instance as positive pairs  $(y_i^a, y_i^b)$ , and treat all others as negative pairs. To calculate the contrastive learning loss for the cluster-based contrastive learning loss, denoted as  $\mathcal{L}_{\text{cluster}_i}^k$ , we use the InfoNCE loss function, represented as follows:

$$-\log \frac{\exp(s(y_i^a, y_i^b)/\tau)}{\sum_{j=1}^M [\exp(s(y_i^k, y_j^k)/\tau) + \exp(s(y_i^a, y_j^b)/\tau)]} \quad (11)$$

where  $M$  represents the number of possible clusters, which is 2 (sensitivity and resistance) in this paper. The cluster-based contrastive learning loss is computed by iterating over all clusters:

$$\mathcal{L}_{\text{cluster}} = \frac{1}{2M} \sum_{i=1}^M (\mathcal{L}_{\text{cluster}_i}^a, \mathcal{L}_{\text{cluster}_i}^b) - H(y) \quad (12)$$

The entropy of the cluster assignment probabilities  $P(y_i^k) = \sum_{i=1}^N (y_i^k / \sum_{i=1}^N y_i^k)$ , where  $k \in \{a, b\}$ , for a mini-batch under each data augmentation is denoted by  $H(Y) = -\sum_{i=1}^M [P(y_i^a) \log P(y_i^a) + P(y_i^b) \log P(y_i^b)]$ . This term is included to prevent the trivial solution of assigning most instances to the same cluster [37].

**4) Joint Learning:** The instance-based contrastive learning paradigm and the cluster-based contrastive learning paradigm operate as two end-to-end learning processes optimized concurrently in a single stage. The overall global contrastive learning loss is defined as follows:

$$\mathcal{L} = \mathcal{L}_{\text{instance}} + \lambda \mathcal{L}_{\text{cluster}} \quad (13)$$

Here,  $\lambda$  is a balancing parameter used to control the relative importance of the two losses during training.

Following unsupervised training, we employ a decoder to reconstruct the fused features of cell lines, which are then utilized for subsequent prediction tasks. The reconstruction of the fused features is performed using the following equation:

$$E_{\text{cellline}} = \text{decoder}(X) \quad (14)$$

Here,  $X$  represents the concatenated vector of the four multi-omics features,  $\text{decoder}(\cdot)$  denotes the decoder, and in this study, we employ an autoencoder for this purpose.

### D. Prediction Module

Once the embeddings of drugs and cell lines are obtained, we concatenate these two embeddings and employ a multilayer perceptron (MLP) to predict the IC50 values of cell line-drug pairs using the following equation:

$$\hat{y}_{i,j} = \sigma((E_{\text{drug}_i} || E_{\text{cellline}_j}) \cdot W_1 + b_1) \cdot W_2 + b_2 \quad (15)$$

Here,  $\hat{y}_{i,j}$  represents the predicted IC50 value for cell line  $j$  and drug  $i$ . The operation  $(\cdot || \cdot)$  denotes the concatenation of two vectors.  $W_1$ ,  $W_2$ ,  $b_1$ , and  $b_2$  are trainable parameters. The symbol  $\sigma$  represents a nonlinear activation function, and in this study, we utilized the Rectified Linear Unit (ReLU) activation function.

### E. Optimization

In the optimization stage, we focus on optimizing the parameters of the drug feature extraction module and the prediction module, while the cell line feature extraction module is independently optimized using the unsupervised learning method. For the regression task, we employ the Mean Squared Error (MSE) loss, which serves as the optimization objective, given by:

$$\mathcal{L}_{\text{regression}} = \frac{1}{N} \sum_{i=1}^N (y_i - \hat{y}_i)^2 \quad (16)$$

Here,  $N$  denotes the total number of cell line-drug pairs in the dataset.  $y_i$  represents the true IC50 value for the  $i$ -th pair, and  $\hat{y}_i$  represents the corresponding predicted IC50 value.

For the classification task, we utilize the Binary Cross Entropy (BCE) loss, which is suitable for binary classification, and formulate the optimization objective as follows:

$$\mathcal{L}_{\text{classification}} = -\frac{1}{N} \sum_{i=1}^N [y_i \log(p_i) + (1 - y_i) \log(1 - p_i)] \quad (17)$$

In this equation,  $N$  represents the number of samples in the batch.  $y_i$  is the true binary label (either 0 or 1) for the  $i$ -th sample, and  $p_i$  is the predicted probability of the positive class for the  $i$ -th sample.

By using the appropriate loss function based on the task at hand, we aim to optimize the model parameters and improve its performance in both regression and classification tasks.

## IV. EXPERIMENTS AND RESULTS

### A. Comparative Experiment

To thoroughly evaluate the efficacy of DeepFusionCDR, we performed an in-depth comparative study against two fundamental methodologies and two cutting-edge techniques designed for cancer drug response prediction. This assessment included both classification and regression tasks. For the regression assessment, we used three prevalent metrics: Pearson's correlation coefficient (PCC), Spearman's correlation coefficient (SCC), and root mean squared error (RMSE). PCC quantifies the linear correlation between observed and predicted IC50 values, SCC reveals the non-parametric rank correlation, and RMSE directly measures the deviation between observed and predicted IC50

**TABLE I**  
EXPERIMENTAL RESULTS ON REGRESSION TASKS

	RMSE	PCC	SCC
SVM	2.7919	0.2782	0.3277
MLP	2.1384	0.5000	0.3679
GraphCDR	1.3321	0.8748	0.8472
DeepTTA	1.2355	0.9032	0.8644
<b>DeepFusionCDR</b>	<b>1.1259</b>	<b>0.9187</b>	<b>0.8864</b>

The bold values represent the best-performing values.

values. For the classification assessment, we implemented two commonly used metrics: the area under the curve (AUC) and the area under the precision-recall curve (AUPR).

We benchmarked our proposed technique, DeepFusionCDR, against the following baseline strategies:

- **SVM** [18]: Support Vector Machine (SVM) is a flexible machine learning algorithm proficient in executing classification and regression tasks. It operates by discerning an optimal hyperplane to segregate classes in a high-dimensional feature space and uses kernel functions to manage nonlinear relationships.
- **MLP** [38]: Multi-Layer Perceptron (MLP) is a versatile neural network model comprising multiple layers of interconnected artificial neurons. It allows for non-linear transformations and hierarchical feature learning, providing proficient solutions to a variety of classification and regression problems via signal propagation and activation functions.
- **GraphCDR** [21]: GraphCDR is a method based on graph neural networks (GNNs) that integrates contrastive learning to enhance the accuracy of cancer drug response prediction. It leverages the graph structure of molecular data to capture intricate relationships and improves representation learning through contrastive learning.
- **DeepTTA** [23]: DeepTTA integrates a transformer-based drug representation learning strategy with a multilayer neural network for predicting anti-cancer drug responses based on transcriptomic data. The model uses transcriptomic gene expression data and chemical substructures of drugs to provide accurate drug response predictions.

For the regression task, the experimental results are consolidated in Table I. The table highlights that DeepFusionCDR outclasses the alternative methods by achieving superior PCC and SCC scores and exhibiting a lower RMSE. Specifically, DeepFusionCDR exceeds the runner-up method in terms of PCC by 1.55% and SCC by 2.2%, and its RMSE score is 0.1096 lower.

For a more tangible evaluation of DeepFusionCDR's regression performance, four distinct cell lines were arbitrarily selected from the test set. DeepFusionCDR was used to predict the IC50 scores for these cell lines in relation to other drugs in the test set. A scatter plot was then generated, with the observed IC50 values on the x-axis and the predicted IC50 values on the y-axis, as depicted in Fig. 2. Similarly, four unique drugs were randomly chosen, and their corresponding scatter plots were illustrated in Fig. 3. The scatter plots in Figs. 2 and 3

**TABLE II**  
EXPERIMENTAL RESULTS ON CLASSIFICATION TASKS

	1:1		1:5		1:10	
	AUC	AUPR	AUC	AUPR	AUC	AUPR
SVM	0.7916	0.7992	0.7925	0.9452	0.7882	0.9699
MLP	0.7690	0.7651	0.7530	0.9282	0.7838	0.9678
GraphCDR	0.8350	0.8370	0.8327	0.9521	0.8279	0.9740
DeepTTA	0.8248	0.8356	0.8249	0.9625	0.8399	0.9787
<b>DeepFusionCDR</b>	<b>0.8531</b>	<b>0.8663</b>	<b>0.8420</b>	<b>0.9626</b>	<b>0.8491</b>	<b>0.9805</b>

The bold values represent the best-performing values.

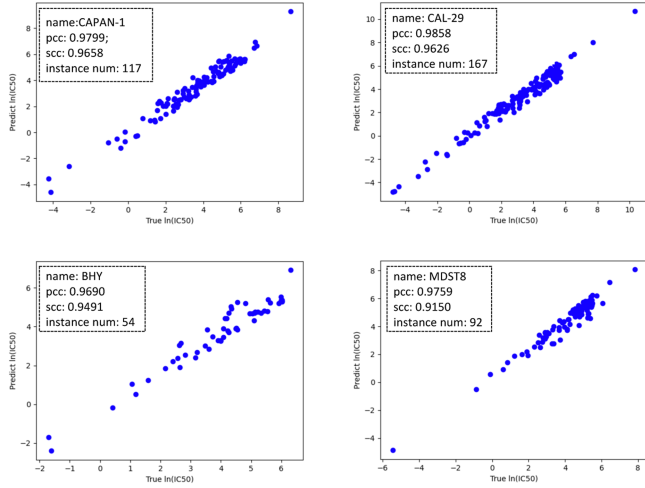


**Fig. 2.** The performance of DeepFusionCDR across different cell lines. The horizontal axis represents the actual IC50 values, and the vertical axis represents the predicted IC50 values.

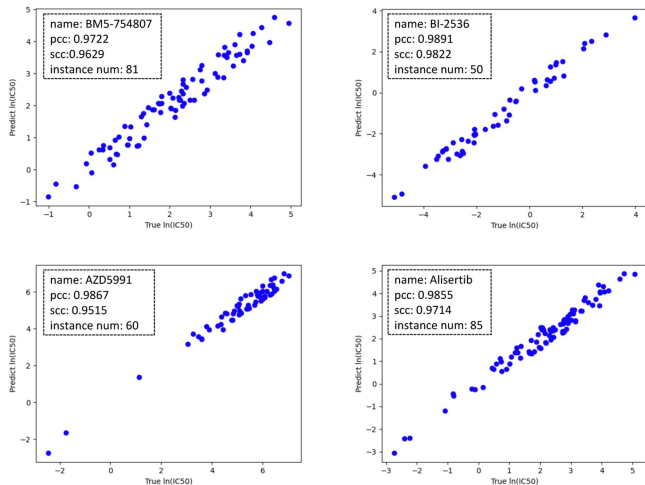


**Fig. 3.** The performance of DeepFusionCDR across different drugs. The horizontal axis represents the actual IC50 values, and the vertical axis represents the predicted IC50 values.

showcase the exceptional regression performance exhibited by DeepFusionCDR.

The scatter plots offer a graphical depiction of the correlation between predicted and observed IC50 values, underscoring the precision and efficacy of DeepFusionCDR in regression tasks.

This form of visual representation bolsters our faith in the predictive proficiency of DeepFusionCDR and affirms its supremacy in accurately forecasting drug responses.

For the classification task, we assembled three datasets with class ratios of 1:1, 1:5, and 1:10. The experimental outcomes are consolidated in Table II. Additionally, we plotted Receiver Operating Characteristic (ROC) and Precision-Recall (PR) curves for each dataset, depicted in Fig. 4(a), (b) and (c) and Fig. 4(d), (e) and (f).

As clearly demonstrated in Table II, DeepFusionCDR attains the highest Area Under the Curve (AUC) and Area Under the Precision-Recall Curve (AUPR) scores across all three datasets. In detail, on the 1:1 dataset, DeepFusionCDR exceeds the second-best method by 1.81% in terms of AUC and 2.93% in terms of AUPR. On the 1:5 dataset, DeepFusionCDR's AUC surpasses that of the second-best method by 0.93%, and its AUPR is superior by 0.01%. Likewise, on the 1:10 dataset, DeepFusionCDR's AUC outperforms the second-best method by 0.92%, and its AUPR is superior by 0.18%.

These experimental findings establish that DeepFusionCDR not only exhibits exemplary classification performance but also showcases robustness. The model persistently achieves superior AUC and AUPR scores across varying class ratios, signaling its competence in accurately discriminating between distinct drug response classes. Furthermore, the robustness of DeepFusionCDR emphasizes its general applicability and effectiveness in real-world scenarios featuring imbalanced class distributions. The ROC and AUPR curves illustrated in Fig. 4(a) and (b) visually affirm the outstanding classification performance of DeepFusionCDR across the three datasets. Altogether, these results substantiate the superiority and dependability of DeepFusionCDR in classification tasks.

DeepFusionCDR has achieved SOTA predictive performance in both classification and regression tasks. We hypothesize that this success can be attributed, in part, to our employment of unsupervised methods for preprocessing multi-omics data, effectively realizing the fusion of multi-omics features. On the other hand, the integration of molecular knowledge through a transformer architecture plays a pivotal role in acquiring embeddings for drug molecules. The combination of these two strategies ultimately leads to exceptionally good predictive outcomes

### B. Predicting on Cancer Patients

To demonstrate the superior capability of the DeepFusionCDR method in predicting drug responses in clinical cancer

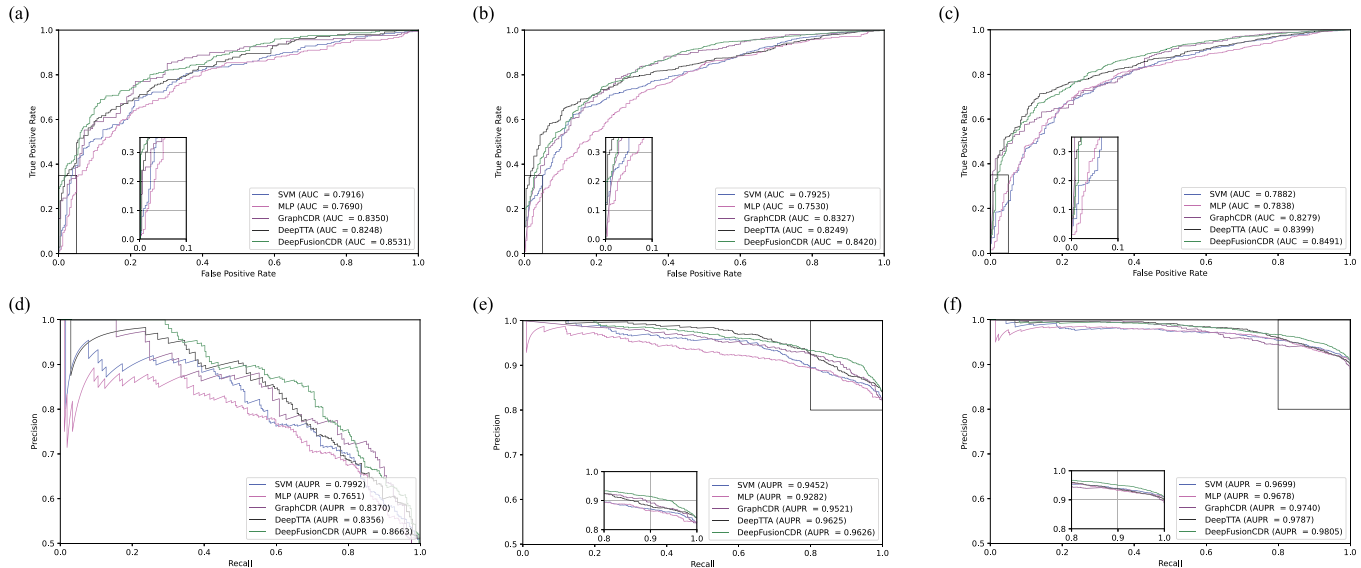


**Fig. 4.** ROC curves and PR curves for datasets with different positive and negative sample ratios. (a), (b), and (c) represent the ROC curves for the 1:1, 1:5, and 1:10 datasets, respectively; (d), (e), and (f) represent the PR curves for the 1:1, 1:5, and 1:10 datasets, respectively.

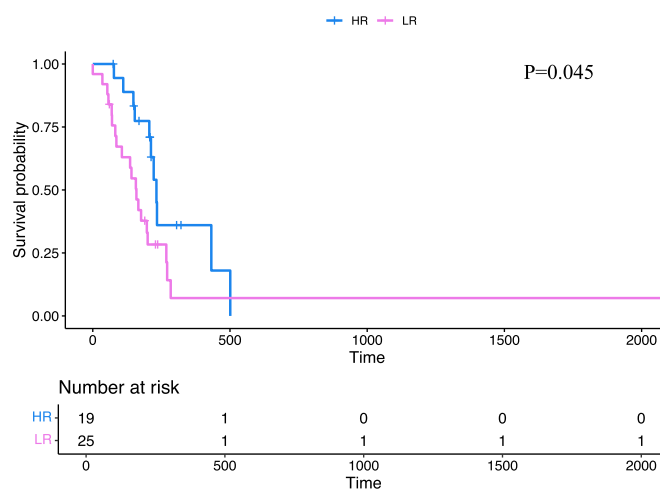


**Fig. 5.** The survival analysis by TCGA patients data with Cisplatin treatment.

patients [39], we meticulously selected patients from the TCGA database who were treated with Cisplatin, including only those with comprehensive clinical and omics data. The clinical data encompassed drug response metrics, Overall Survival (OS) days, and OS status, while the omics data included mutations, CNV, mRNA expression, and DNA methylation profiles. The diseases treated encompassed Stomach Adenocarcinoma (STAD), Pancreatic Adenocarcinoma (PAAD), Liver Hepatocellular Carcinoma (LIHC), and Esophageal Carcinoma (ESCA). Ultimately, data from 44 clinical patients were collected. We utilized the trained DeepFusionCDR to predict outcomes based on the clinical data and constructed the associated survival analysis curves, as illustrated in Fig. 5. As depicted in Fig. 5, the subgroup of samples treated with Cisplatin that had a high predicted response to the drug demonstrated significantly better survival

outcomes ( $P = 0.045$ ) compared to those with a low predicted response.

### C. Ablation Experiment

To explore the roles of different components within the DeepFusionCDR framework, we conducted a series of ablation experiments. For a clear representation of the influence of individual omics features on DeepFusionCDR's performance, we produced a histogram, as depicted in Fig. 6. The horizontal axes of these histograms represent the use of CNV features (CNV), methylation features (ME), mutation features (MU), and transcriptomics (TR) features, respectively. Fig. 6(a) signifies the RMSE, PCC and SCC value of DeepFusionCDR with respect to different omics features. The RMSE is displayed on the right Y-axis, whereas the PCC and SCC are illustrated on the left Y-axis. and Fig. 6(b) showcases the AUC and AUPR values of DeepFusionCDR in the presence of differing omics features.

Our experimental findings conclusively reveal the advantageous impact of integrating multi-omic features on both classification and regression tasks in most instances. This underscores the beneficial effect of harnessing multi-omics data to improve experimental performance. However, we also encountered situations where this integration yielded unfavorable results. For example, when comparing the use of all four omics features with the individual use of any two or three, we observed higher RMSE values. This suggests that merely concatenating each feature fails to effectively characterize cell lines. Importantly, the introduction of contrastive learning has substantially improved the performance across all DeepFusionCDR indicators, underscoring the essential role of this learning approach in effectively fusing multi-omics feature data.

Subsequently, we validated the roles of two important contrastive learning paradigm constructed in the fusion of multi-omics features: cluster-based contrastive learning paradigm and

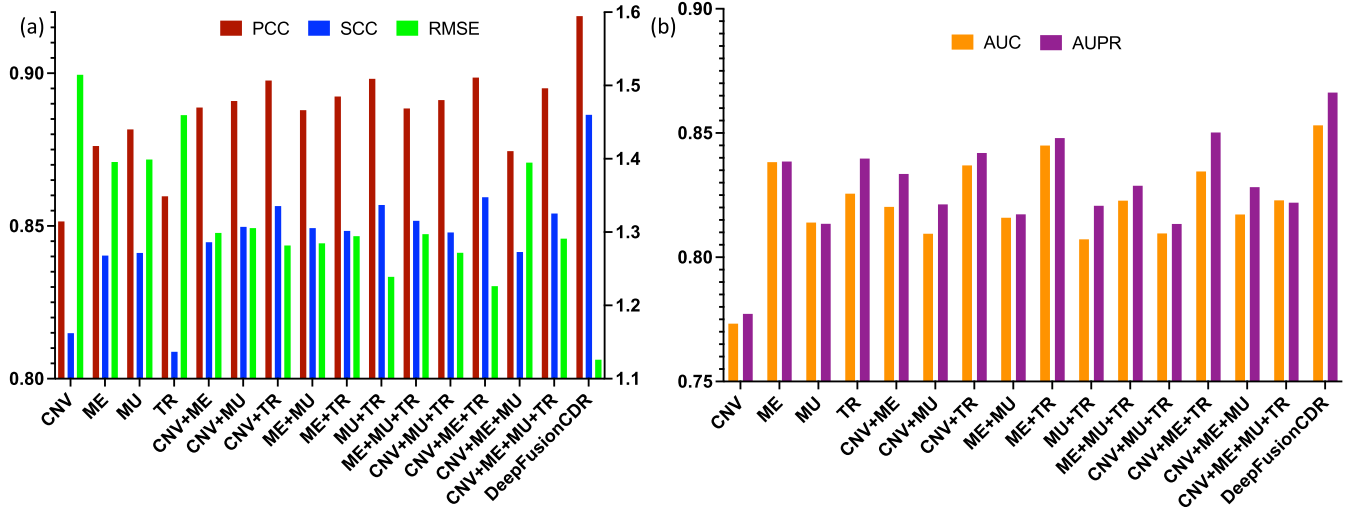


**Fig. 6.** Results of multi-omics data ablation experiments. (a) displays the experimental results of using different omics data in regression tasks, where RMSE is represented using the right y-axis, and PCC and SCC are represented using the left y-axis. (b) shows the results of using different omics data in classification tasks.

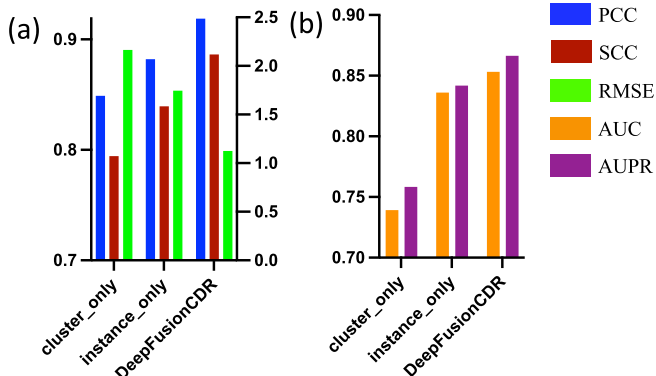


**Fig. 7.** Experimental results on the impact of different contrastive learning paradigm on the performance of DeepFusionCDR. (a) shows the experimental results of using different contrastive learning paradigm in regression tasks. (b) shows the results of using different contrastive learning paradigm in classification tasks.

instance-based contrastive learning paradigm. We developed two distinct variants, cluster\_only, which exclusively utilizes the cluster-based contrastive learning paradigm, and instance\_only, which solely employs the instance-based contrastive learning paradigm. The experimental results are illustrated in Fig. 7. From Fig. 7, it is evident that using only a single contrastive learning optimization objective results in decreased model performance, whereas combining both contrastive learning objectives enables the model to achieve optimal performance.

Furthermore, to visually analyze the distribution of fused cell line features over different epochs, we applied t-distributed stochastic neighbor embedding (t-SNE), as shown in Fig. 8. Fig. 8(a) presents the results derived from applying t-SNE dimensionality reduction to the initial cell line features. Fig. 8(b) then depicts the distribution of cell line features post-training, while Fig. 8(c) shows the distribution following an extensive number of training epochs, indicating model overfitting. When

we implemented unsupervised contrastive learning training, we found that the fused feature representation of cell lines showed strong discriminatory capabilities. This leads us to hypothesize that the fused features of cell lines, after training, might carry potential resistance or sensitivity labels, which could be valuable for future predictive tasks.

#### D. Predicting Missing CDRs

To predict the missing Cancer Drug Responses (CDRs) in the database, we employed DeepFusionCDR, which was trained using all the available 124,135 cell line-drug pairs in the database. Following this, we used this model to predict the remaining 14,045 missing CDRs. Fig. 9 presents both the lowest and highest ten mean IC50 value drugs, arranged based on the average IC50 value of each drug. The resulting predictions indicate a substantial potential of these drugs for cancer treatment.

Among the drugs identified, Romidepsin was the most effective. Romidepsin is an FDA-approved HDAC inhibitor used for treating refractory cutaneous T-cell lymphoma (CTCL). It increases histone acetylation levels by inhibiting histone deacetylase (HDAC), influencing gene expression and cell cycle regulation. This eventually leads to apoptosis and cell cycle arrest in tumor cells [40], [41].

Our model also identified Bortezomib as a notably potent drug. Bortezomib is an effective proteasome inhibitor that exhibits significant anti-tumor potential in solid tumors and hematological malignancies [42]. Its action mechanism involves the inhibition of NF- $\kappa$ B activation, promoting increased apoptosis and reduced production of angiogenic cytokines. With remarkable in vitro activity, Bortezomib is currently under investigation in clinical trials for various cancer types, including multiple myeloma, lymphomas, leukemia, head and neck cancer, gastrointestinal cancers, colorectal cancer, prostate cancer, and non-small cell lung cancer [43].

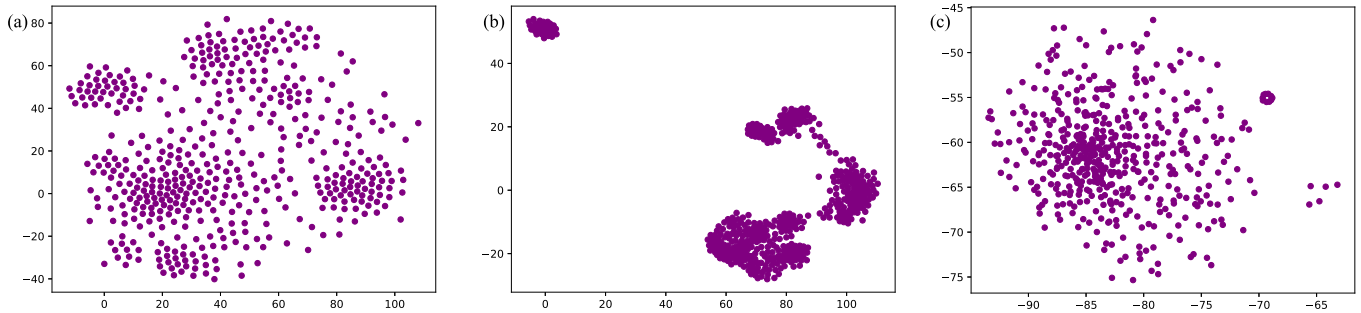


**Fig. 8.** The visualization of the fused cell line feature over training epochs are presented in this figure. (a) represents the distribution of cell line features before training, while (b) illustrates the distribution after training. Finally, (c) highlights the feature distribution following an extended period of training epochs.

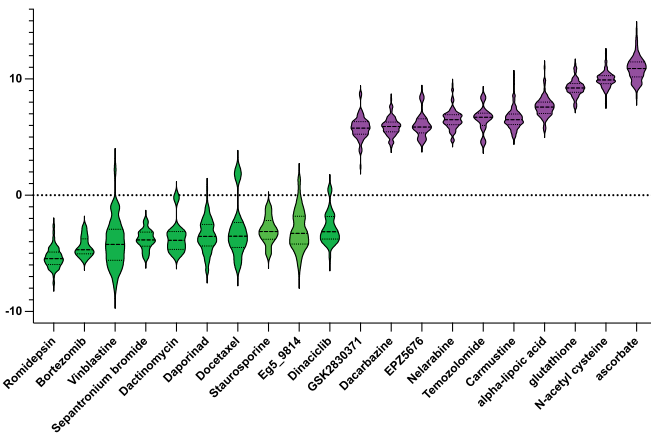


**Fig. 9.** Prediction of missing CDRs and ranking of drugs based on mean IC50 values. The figure presents the top ten and bottom ten drugs, ranked by their predicted mean IC50 values.

Furthermore, Vinblastine was successfully pinpointed as the third most effective drug by our predictions. This chemotherapy medication has shown effectiveness in treating various forms of cancer, including lymphoma, ovarian cancer, and breast cancer. It works by inhibiting the polymerization of microtubules, disrupting cell division and proliferation [44].

### E. Case Study

Prostate cancer, predominant among men aged 45 to 60, especially in Western countries, poses significant health threats [45], [46]. The existing therapeutic interventions for prostate cancer often present limitations such as modest efficacy, prohibitive costs, severe side effects, and the development of drug resistance [47], [48], [49]. This underscores the necessity for continued exploration of optimally effective drugs to combat prostate cancer.

To ascertain the practical applicability of DeepFusionCDR, we utilized the trained model to predict the in vitro IC50 values of drugs for prostate cancer treatment. We first excluded prostate cancer-related therapeutic drugs with true IC50 labels from the GDSC dataset. The remaining drugs were then ranked by their predicted IC50 value within the same cell line. We scrutinized the top and bottom ten drug pairs, based on the lowest scores,

**TABLE III**  
THE 10 DRUGS WITH THE LOWEST PROSTATE CANCER-RELATED SCORES

drug	Pubmed id
Romidepsin	19608618
Dactinomycin	unknown
Bortezomib	34645397, 30720063
Vinblastine	23138870
Vinorelbine	15520061
Rapamycin	27648364
Methotrexate	27654169
Docetaxel	22811914
Daporinad	33349973
Separantrium bromide	unknown

to further analyze drug sensitivity. Our predictions were then cross-verified against existing literature.

Detailed descriptions of several potential drugs are provided in Table III. Romidepsin, an FDA-approved HDAC inhibitor for cutaneous T-cell lymphoma treatment, has shown promise in eliminating androgen receptor signaling in prostate cancer treatment. Phase II clinical trials have reported specific effects of Romidepsin in prostate cancer progression, marking it as a potential anti-prostate cancer drug [50]. Bortezomib, a 26S proteasome inhibitor, has demonstrated efficacy in treating hematologic malignancies. Numerous studies indicate that Bortezomib can augment its anti-tumor impact by inhibiting the Wnt/β-Catenin signaling pathway in prostate cancer cells and inducing cell death by suppressing androgen receptor expression [51], [52]. Vinblastine, a standard component in many chemotherapy regimens, is used to treat various tumors, including Hodgkin's lymphoma and lung cancer. It has been confirmed to exert potent cytotoxic effects on prostate cancer cell lines [53]. Moreover, among the top ten ranked drugs, two have not yet been confirmed to inhibit prostate cancer cell proliferation, warranting further investigation.

### V. DISCUSSION AND CONCLUSION

In conclusion, our study presents DeepFusionCDR, a novel deep learning methodology that integrates multi-omics fusion and molecular-specific transformers to predict cancer drug responses. Evaluations conducted on the GDSC dataset illustrate that DeepFusionCDR surpasses existing methodologies in both

regression and classification tasks. These findings underscore the potential of DeepFusionCDR to enhance personalized cancer treatment strategies by leveraging comprehensive multi-omics data. Although DeepFusionCDR has demonstrated significant predictive success, it is not without its inherent limitations. Initially, our predictive analyses were confined to the reactions of single cell lines to individual drugs, thereby failing to consider the potential synergistic effects of combination therapies, which are increasingly recognized within contemporary cancer treatment paradigms. Furthermore, the analysis conducted by DeepFusionCDR was limited to four types of omics data. Due to the instability and challenges in accessing data, important datasets such as proteomics [54], [55] were not included in the study, despite their critical role in the drug discovery process. In the future, we plan to gather more stable proteomics data and consider the incorporation of transfer learning strategies to further enhance the predictive performance and interpretability of our model.

### ACKNOWLEDGMENT

We are grateful for resources from the High Performance Computing Center of Central South University. We thank the TCGA Research Network for making the TCGA data available to the research community.

### REFERENCES

- [1] W. Cao, H.-D. Chen, Y.-W. Yu, N. Li, and W.-Q. Chen, "Changing profiles of cancer burden worldwide and in China: A secondary analysis of the global cancer statistics 2020," *Chin. Med. J.*, vol. 134, no. 07, pp. 783–791, 2021.
- [2] J. Barretina et al., "The cancer cell line encyclopedia enables predictive modelling of anticancer drug sensitivity," *Nature*, vol. 483, no. 7391, pp. 603–607, 2012.
- [3] W. Yang et al., "Genomics of drug sensitivity in cancer (GDSC): A resource for therapeutic biomarker discovery in cancer cells," *Nucleic acids Res.*, vol. 41, no. D1, pp. D955–D961, 2012.
- [4] Y.-C. Chiu et al., "Deep learning of pharmacogenomics resources: Moving towards precision oncology," *Brief. Bioinf.*, vol. 21, no. 6, pp. 2066–2083, 2020.
- [5] Q. Liu, Z. Hu, R. Jiang, and M. Zhou, "DeepCDR: A hybrid graph convolutional network for predicting cancer drug response," *Bioinformatics*, vol. 36, no. Supplement\_2, pp. i911–i918, 2020.
- [6] H. Sharifi-Noghabi, O. Zolotareva, C. C. Collins, and M. Ester, "MOLI: Multi-omics late integration with deep neural networks for drug response prediction," *Bioinformatics*, vol. 35, no. 14, pp. i501–i509, 2019.
- [7] Y. Chang et al., "Cancer drug response profile scan (CDRscan): A deep learning model that predicts drug effectiveness from cancer genomic signature," *Sci. Rep.*, vol. 8, no. 1, 2018, Art. no. 8857.
- [8] P. Liu, H. Li, S. Li, and K.-S. Leung, "Improving prediction of phenotypic drug response on cancer cell lines using deep convolutional network," *BMC Bioinf.*, vol. 20, no. 1, pp. 1–14, 2019.
- [9] M. Cieslik and A. M. Chinaiyan, "Cancer transcriptome profiling at the juncture of clinical translation," *Nature Rev. Genet.*, vol. 19, no. 2, pp. 93–109, 2018.
- [10] J.-J. Chen, S. Knudsen, W. Mazin, J. Dahlgaard, and B. Zhang, "A 71-gene signature of TRAIL sensitivity in cancer cells," *Mol. Cancer Therapeutics*, vol. 11, no. 1, pp. 34–44, 2012.
- [11] A. Rosenwald et al., "The proliferation gene expression signature is a quantitative integrator of oncogenic events that predicts survival in mantle cell lymphoma," *Cancer Cell*, vol. 3, no. 2, pp. 185–197, 2003.
- [12] S. Ramaswamy, K. N. Ross, E. S. Lander, and T. R. Golub, "A molecular signature of metastasis in primary solid tumors," *Nature Genet.*, vol. 33, no. 1, pp. 49–54, 2003.
- [13] A. H. Bild et al., "Oncogenic pathway signatures in human cancers as a guide to targeted therapies," *Nature*, vol. 439, no. 7074, pp. 353–357, 2006.
- [14] N. Zhang, H. Wang, Y. Fang, J. Wang, X. Zheng, and X. S. Liu, "Predicting anticancer drug responses using a dual-layer integrated cell line-drug network model," *PLoS Comput. Biol.*, vol. 11, no. 9, 2015, Art. no. e1004498.
- [15] T. Turki and Z. Wei, "A link prediction approach to cancer drug sensitivity prediction," *BMC Syst. Biol.*, vol. 11, pp. 1–14, 2017.
- [16] F. Zhang, M. Wang, J. Xi, J. Yang, and A. Li, "A novel heterogeneous network-based method for drug response prediction in cancer cell lines," *Sci. Rep.*, vol. 8, no. 1, pp. 1–9, 2018.
- [17] P. Geeleher, N. J. Cox, and R. S. Huang, "Clinical drug response can be predicted using baseline gene expression levels and in vitro drug sensitivity in cell lines," *Genome Biol.*, vol. 15, pp. 1–12, 2014.
- [18] Z. Dong et al., "Anticancer drug sensitivity prediction in cell lines from baseline gene expression through recursive feature selection," *BMC Cancer*, vol. 15, no. 1, pp. 1–12, 2015.
- [19] A. Daemen et al., "Modeling precision treatment of breast cancer," *Genome Biol.*, vol. 14, pp. 1–14, 2013.
- [20] M. P. Menden et al., "Machine learning prediction of cancer cell sensitivity to drugs based on genomic and chemical properties," *PLoS one*, vol. 8, no. 4, 2013, Art. no. e61318.
- [21] X. Liu, C. Song, F. Huang, H. Fu, W. Xiao, and W. Zhang, "GraphCDR: A graph neural network method with contrastive learning for cancer drug response prediction," *Brief. Bioinf.*, vol. 23, no. 1, 2022, Art. no. bbab457.
- [22] K. Huang, C. Xiao, L. Glass, and J. Sun, "Explainable substructure partition fingerprint for protein, drug, and more," in *Proc. NeurIPS Learn. Meaningful Representation Life Workshop*, 2019.
- [23] L. Jiang, C. Jiang, X. Yu, R. Fu, S. Jin, and X. Liu, "Deeptta: A transformer-based model for predicting cancer drug response," *Brief. Bioinf.*, vol. 23, no. 3, 2022, Art. no. bbac100.
- [24] A. Vaswani et al., "Attention is all you need," in *Proc. Adv. Neural Inf. Process. Syst.*, vol. 30, 2017.
- [25] M. H. Segler, T. Kogej, C. Tyrchan, and M. P. Waller, "Generating focused molecule libraries for drug discovery with recurrent neural networks," *ACS Central Sci.*, vol. 4, no. 1, pp. 120–131, 2018.
- [26] R. Gómez-Bombarelli et al., "Automatic chemical design using a data-driven continuous representation of molecules," *ACS Central Sci.*, vol. 4, no. 2, pp. 268–276, 2018.
- [27] S. Jastrzebski, D. Lesniak, and W. M. Czarnecki, "Learning to SMILE(S)," 2016, *arXiv:1602.06289*.
- [28] P. W. Battaglia et al., "Relational inductive biases, deep learning, and graph networks," 2018, *arXiv:1806.01261*.
- [29] J.-B. Grill et al., "Bootstrap your own latent-a new approach to self-supervised learning," in *Proc. Adv. Neural Inf. Process. Syst.*, 2020, vol. 33, pp. 21271–21284.
- [30] T. Chen, S. Kornblith, M. Norouzi, and G. Hinton, "A simple framework for contrastive learning of visual representations," in *Proc. Int. Conf. Mach. Learn.*, 2020, pp. 1597–1607.
- [31] J. Li, P. Zhou, C. Xiong, and S. C. Hoi, "Prototypical contrastive learning of unsupervised representations," in *Proc. Int. Conf. Learn. Representations*, 2021. [Online]. Available: <https://openreview.net/forum?id=KmykpuSrqc>
- [32] T. Gao, X. Yao, and D. Chen, "SimCSE: Simple contrastive learning of sentence embeddings," in *Proc. 2021 Conf. Empirical Methods Natural Lang. Process.*, M.-F. Moens, X. Huang, L. Specia, and S. W.-t. Yih, Eds. Punta Cana, Dominican Republic, Nov. 2021, pp. 6894–6910. [Online]. Available: <https://aclanthology.org/2021.emnlpmain.552>
- [33] Y.-S. Chuang et al., "DiffCSE: Difference-based contrastive learning for sentence embeddings," in *Proc. 2022 Conf. North Amer. Chapter Assoc. Comput. Linguistics: Human Lang. Technol.*, M. Carpuat, M.-C. de Marneffe, and I. V. Meza Ruiz, Eds. Seattle, United States, Jul. 2022, pp. 4207–4218. [Online]. Available: <https://aclanthology.org/2022.naacl-main.311>
- [34] Y. Li, G. Qiao, X. Gao, and G. Wang, "Supervised graph co-contrastive learning for drug-target interaction prediction," *Bioinformatics*, vol. 38, no. 10, pp. 2847–2854, 2022.
- [35] C.-H. Yeh, C.-Y. Hong, Y.-C. Hsu, T.-L. Liu, Y. Chen, and Y. LeCun, "Decoupled contrastive learning," in *Proc. 17th Eur. Conf. Comput. Vis.*, 2022, pp. 668–684.
- [36] Y. Li, P. Hu, Z. Liu, D. Peng, J. T. Zhou, and X. Peng, "Contrastive clustering," in *Proc. AAAI Conf. Artif. Intell.*, 2021, vol. 35, pp. 8547–8555.
- [37] W. Hu, T. Miyato, S. Tokui, E. Matsumoto, and M. Sugiyama, "Learning discrete representations via information maximizing self-augmented training," in *Proc. Int. Conf. Mach. Learn.*, 2017, pp. 1558–1567.

- [38] J. Choi, S. Park, and J. Ahn, "RefDNN: A reference drug based neural network for more accurate prediction of anticancer drug resistance," *Sci. Rep.*, vol. 10, no. 1, 2020, Art. no. 1861.
- [39] J. N. Weinstein et al., "The cancer genome atlas pan-cancer analysis project," *Nature Genet.*, vol. 45, no. 10, pp. 1113–1120, Oct. 2013.
- [40] M. Duvic et al., "Phase 2 trial of oral vorinostat (suberoylanilide hydroxamic acid, SAHA) for refractory cutaneous T-cell lymphoma (CTCL)," *Blood*, vol. 109, no. 1, pp. 31–39, 2007.
- [41] R. L. Piekarsz et al., "Phase II multi-institutional trial of the histone deacetylase inhibitor romidepsin as monotherapy for patients with cutaneous T-cell lymphoma," *J. Clin. Oncol.*, vol. 27, no. 32, 2009, Art. no. 5410.
- [42] P. G. Richardson et al., "A phase 2 study of bortezomib in relapsed, refractory myeloma," *New England J. Med.*, vol. 348, no. 26, pp. 2609–2617, 2003.
- [43] A. M. Roccaro, A. Vacca, and D. Ribatti, "Bortezomib in the treatment of cancer," *Recent Patents Anti-cancer Drug Discov.*, vol. 1, no. 3, pp. 397–403, 2006.
- [44] L. Caputi et al., "Missing enzymes in the biosynthesis of the anticancer drug vinblastine in Madagascar periwinkle," *Science*, vol. 360, no. 6394, pp. 1235–1239, 2018.
- [45] W. I. Luining et al., "Targeting PSMA revolutionizes the role of nuclear medicine in diagnosis and treatment of prostate cancer," *Cancers*, vol. 14, no. 5, 2022, Art. no. 1169.
- [46] C. H. Pernar, E. M. Eböt, K. M. Wilson, and L. A. Mucci, "The epidemiology of prostate cancer," *Cold Spring Harbor Perspectives Med.*, vol. 8, no. 12, 2018, Art. no. a030361.
- [47] S. Gillessen et al., "Management of patients with advanced prostate cancer—metastatic and/or castration-resistant prostate cancer: Report of the advanced prostate cancer consensus conference (apccc) 2022," *Eur. J. Cancer*, vol. 185, pp. 178–215, 2023.
- [48] M. Sekhoacha, K. Riet, P. Motloung, L. Gumenku, A. Adegoke, and S. Mashele, "Prostate cancer review: Genetics, diagnosis, treatment options, and alternative approaches," *Molecules*, vol. 27, no. 17, 2022, Art. no. 5730.
- [49] C. Herberts et al., "Deep whole-genome ctDNA chronology of treatment-resistant prostate cancer," *Nature*, vol. 608, no. 7921, pp. 199–208, 2022.
- [50] L. Molife et al., "Phase II, two-stage, single-arm trial of the histone deacetylase inhibitor (HDACI) romidepsin in metastatic castration-resistant prostate cancer (CRPC)," *Ann. Oncol.*, vol. 21, no. 1, pp. 109–113, 2010.
- [51] Y. Zhang et al., "Bortezomib potentiates antitumor activity of mitoxantrone through dampening Wnt/β-catenin signal pathway in prostate cancer cells," *BMC Cancer*, vol. 21, no. 1, pp. 1–10, 2021.
- [52] K. Kuroda and H. Liu, "The proteasome inhibitor, bortezomib, induces prostate cancer cell death by suppressing the expression of prostate-specific membrane antigen, as well as androgen receptor," *Int. J. Oncol.*, vol. 54, no. 4, pp. 1357–1366, 2019.
- [53] B. J. Passer, T. Cheema, S. Wu, C. Wu, S. D. Rabkin, and R. L. Martuza, "Combination of vinblastine and oncolytic herpes simplex virus vector expressing IL-12 therapy increases antitumor and antiangiogenic effects in prostate cancer models," *Cancer Gene Ther.*, vol. 20, no. 1, pp. 17–24, 2013.
- [54] S. Hanash, "Disease proteomics," *Nature*, vol. 422, no. 6928, pp. 226–232, Mar. 2003.
- [55] F. Meissner, J. Geddes-McAlister, M. Mann, and M. Bantscheff, "The emerging role of mass spectrometry-based proteomics in drug discovery," *Nature Rev. Drug Discov.*, vol. 21, no. 9, pp. 637–654, Sep. 2022.